AN OPTIMAL DESIGN OF LLC RESONANT CONVERTER USING FIREFLY ALGORITHM BASED PARAMETER OPTIMIZATION APPROACH

Sarath K S
Hindustan University, Padur, Chennai
sarathksks14@gmail.com

Abstract: The development of power conversion technology is in constant demand due to high power efficiency and high power density. In the resonant converter, huge resonant converter topologies are available and among them, LLC converter is the most attractive one as it is capable of operating in the wide variation range of input voltage and load conditions. Apart from these advantages, LLC Resonant Converter (LLC-RC) suffers from drawbacks like power loss and voltage fluctuations. Thus, this paper intends to develop novel LLC-RC designs on the basis of the Parameter Optimization (PO) algorithm. The proposed model overcomes the major shortcoming by employing a non-conceptual model on the basis of the simulated outcome. The intelligent model is constructed under the start-up conditions with the literary outcomes achieved from the resonant current. As a novelty, the time constant of the resonant converter is optimized by Firefly algorithm (FF). The time constant is optimized on the basis of the objective model, which was obtained from the function of start-up time. The start-up time was diminished and the response speed of the output voltage was increased. Finally, the proposed Firefly algorithm based Parameter Optimization (FF-PO) model was compared with the existing models like Whale Optimization Algorithm based Parameter Optimization (WOA-PO), IAPO, Ant Bee Colony-PO (ABC-PO), Particle Swarm Optimization-PO (PSO-PO) and Grey Wolf Optimization (GWO-PO) on the basis of error and steady-state response.

Keywords: LLC resonant converter; Output voltage; peak value; Parameter optimization; RMSE; Firefly algorithm based Parameter Optimization (FF-PO) model.

1. Introduction

In recent decades, the usage of electricity becomes a rapidly increasing demand for present power supply industry owing to the rise in the requirements in distributed power supply systems [6] [7]. The process of power conversion is to analyze and supply electricity, further, the power converters are required universally to fulfill the electric power demands. Generally, the power conversion is defined as a significant connection among the supplied power source to the consumer electronic devices/energy transmission/storage products. resonant DC/DC converter is a group of converters with L-C resonant tank working as the main role in power conversion technology [8]. Moreover, the basic ideas behind the construction of resonant converters are the circulating energy available in the L-C resonant circuit is controllable through modifying the operating frequency. Thus, the converter is able to control the input power to the required output voltage. Typically, the resonant converters comprised of three basic parts such as rectifier, switch network, and resonant tank. Usually, the resonant tank performs as a frequency selector for an inverter, while in a converter, the sinusoidal waveform purity is not considered as a rectifier and the output low-pass filter can transform the DC from AC. Further, the different resonant properties of the L-C tank decide the various functionalities of the resonant converters [9] [10]. Moreover, the high fluctuations in the resonance intensify the current distributed to the resonant tank that intensifies the conduction losses as well as balance the benefits of short switching losses [11] [12].

Generally, resonant DC/DC converter is a group of converters with L-C resonant tank working as the main role in power conversion technology [13] [15]. Moreover, the basic ideas behind the construction of resonant converters are the circulating energy available in the L-C resonant circuit is controllable through modifying the operating frequency. In L-C resonant tank structure, it has different types which are the L-C resonant tanks [14] [17]. The Series Resonant Converter (SRC) has the resonant inductor and capacitor in series. Further, the resonant tank is connected serially with the output load resistance as well as the resonant tank impedance Z performs as a function to the switching frequency [16] [18]. The major drawback of SRC is high switching loss in MOSFET converters [19] [20]. The Parallel Resonant Converter (PRC) topology ahs the two resonant components (resonant inductor and Capacitor) in parallel. Here, the peak gain is achieved in the lower frequency. The major drawback of PRC is high conduction loss as well as poor efficiency for light load condition. So, with the intention of overriding these drawbacks, the LCC Resonant Converter (Series-Parallel Resonance Converter) is the combination of SRC and PRC. The major advantages of LLC Resonant Converter (LLC-RC) are zero load handling capability under light load condition [21] [22].

In an LLC-RC topology under the Frequency Domain Method, the higher harmonics of the square wave voltage were ignored [23] [29]. This model provides no details on the operation current or voltage behavior of the converter. The state-plane analysis for LLC-RC depicts the relation between state variables like the resonant currents and voltages using the state-plane diagram. The major drawback of this model is multiple resonant stages concerning the DC characteristic information [24] [25]. In the Time Domain Method of LLC-RC, the periodic resonant current, as well as the voltage waveforms, are achieved by sorting the operation modes. The power losses are higher in this technique [26] [27] [28]. Hence, there is a necessity to have an optimal design for LLC-RC.

The major contribution of this research work is to design a novel LLC-RC converter by optimizing the output voltage and resonant inductor current in order to diminish the error. The proposed FF-PO model is compared with the state-of-art models like IA-PO, ABC-PO, PSO-PO, WOA-PO, and GWO-PO in terms of RMSE and steady-state response.

The rest of the paper is organized as: Section 2 provides a compact review on the related works done in LLC-RC design. Section 3 portrays LLC resonant converter model and Section 4 discusses the parameters optimization for the start-up process. The objective of the LLC converter design is depicted in Section 5. The results acquired and their corresponding discussion is provided in Section 6. Section 7 provides a strong conclusion to this research work.

2. Literature Survey

2.1 Related Works

In 2019, Kwon et al. [1] formulated the no-load control method using full-bridge structure in order to achieve the plasma sputtering process in the LLC resonant converter. Initially, the plasma was generated by operating the plasma sputtering process under a no-load condition. On the basis of the parasitic component, the proposed no-load control method was evaluated in order to exhibit the enhancement in the performance of the proposed model.

In 2018, Singh [2] developed a novel HV resonant DC-DC converter in MPM based transmitters with the objective of powering the powering Traveling Wave Tube (TWT). In order to additional voltage boost, the LLC converter was made to operate under series resonant frequency. The Symmetrical Quadrupler Rectifier (SQR) based high voltage LLC resonant was utilized to solve the issues related to the discontinuous secondary current. In the differential modes of operation, the SQR, as well as the LLC resonant full-bridge inverter, were coupled together to achieve additional voltage gain.

In 2012, Madheswaran et al. [3] proposed Digital Signal Processor (DSP) based fuzzy controller for LLC resonant converter with the intention of estimating the output voltage regulation and d and supply voltage fluctuations. The proposed model was analyzed in terms of both closed-loop and open-loop conditions using state-space model. In the proposed model, the output voltage was regulated by the fuzzy controller by means of varying the supply voltage and load disturbance.

In 2019, Hua et al. [4] introduced a Dual-Bridge (DB) LLC resonant converter for dc/dc conversion on the basis of the switch integration technique for a wide range of low input voltage. In the Full-Bridge (FB) LLC and Half-Bridge (HB) LLC, the buck-boost converter was employed in the front stage in order to achieve greater input voltage. In addition to this, the magnetizing inductance was maximized. Further, at different input voltages, the different phase-shift modulation gains were used by DB LLC resonant converter at different input voltages.

In 2018, Yang et al. [5]projected a novel bidirectional LLC-C resonant converter for an energy storage system with the aid of normalized symmetry resonant tank. For each of the resonant capacitor, two auxiliary switches were employed in order to provide bypass path between the capacitors. The proposed model operated either forward or backward operating mode on the basis of the switching.

3. LLC Resonant Converter Model

Among the DC-DC converter like series resonant converter, parallel resonant converter, and series-parallel resonance converter, the most favorable topology is LLC-RC as it has high power density as well as high effectiveness. Apart from the error in LLC-RC is high and several works are being conducted in for a further reduction in the error and enhancement in performance as well as a control mechanism. The control scheme broadly adopted to secure real-time measurement is the frequency modulation control scheme. The frequency of switching is governed by diminishing the linear pattern or exponential pattern from higher frequency to steady-state frequency by the frequency modulation control scheme. The high frequency and steady-state frequency are represented suing the notation f_{HH} and f_{ST}, respectively. The mathematical formula for frequency is exhibited in Eq. (1). The time and the frequency-time constant are denoted as t and τ, respectively. It is easier to execute the exponential outline with a first-order filter and during switching the frequency conversion is smoother. On the other hand, the trial-and-error technique describing τ is wearisome [19], owing to the deficiency in the precise investigation of the dynamic method of the converter. The overall architecture of LLC-RC is shown in Fig.1.

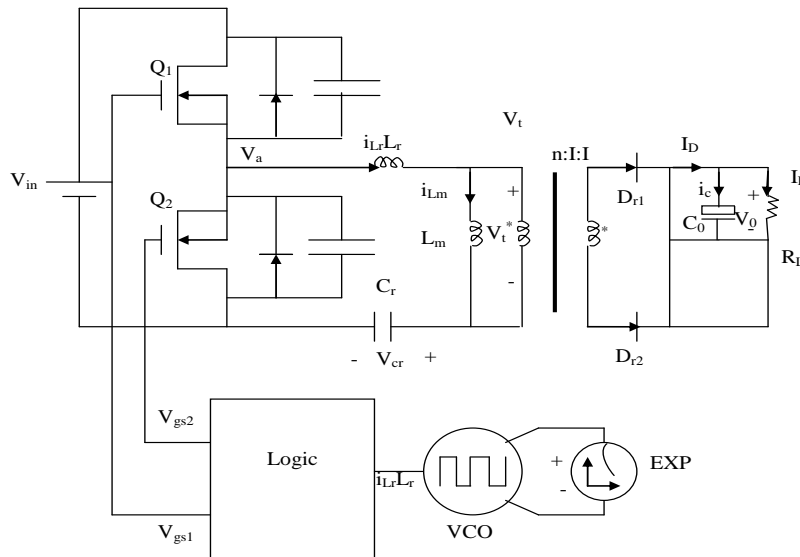$$f = f_{ST} + \left(f_{HH} - f_{ST}\right)e^{\frac{-t}{\tau}} \tag{1}$$

Fig. 1. *Overall architecture of the LLC-Resonant converter*

4. Parameter Optimization for the Startup Process

On the basis of the combined state equations, it is confined that the radius and the center of arc trajectory are closely related to the output voltage. Thus, by measuring the output voltage, the entire state variables involved in the start-up process can be determined.

4.1 Output Voltage

The additional current to load is decreased by charging the capacitor with rectifier current. As the required output is achieved from the capacitor during the switching process, the output voltage is considered to be stable and the essential current flows to load. Eq. (2) depicts the mathematical formula for increased output voltage throughout one rectifier duration. The current through the capacitor is represented as i_c and the sum of the current from two rectifier diodes, load current and output current are denoted using the notation i_D, i_R and C_0, respectively. Further, all throughout a rectifier conduction period under steady-state, the output mean value of capacitor current i_c, as well as the addition of all the

magnetic current, i_{Lm} is symmetrical and equal to zero. Thus, Eq. (2) gets transformed as per Eq. (3). In the rectifier conducting period, the value of the Eq. (4) and Eq. (5) varies from $t1$ to $t3$. The resonant capacitor voltage and the resonant capacitor is V_{C_r} and C_r, respectively. The critical load resistor is denoted using the notation R_L. In addition, the resonant inductor current, resonant impedance and the switching period is represented as i_{Lr}, Z_0 and T_s, respectively. On the basis of these parameters, Eq. (6) and Eq. (7) are formulated. The primary phases at time duration t_1 and t_2 of arc $(x_1, 0)$ and $(x_2, 0)$ are denoted as ϕ_1 and ϕ_2, respectively. The natural frequency is denoted as ω_0 and its corresponding mathematical formula is shown in Eq. (8). As per Eq. (9), the current in the inductor is balanced and here the notation for exciting current is I_{Lm}.

$$\Delta V_0 = \frac{1}{C_0} \int_0^{\frac{T_s}{2}} i_c dt = \frac{1}{C_0} \int_0^{\frac{T_s}{2}} (i_D - i_R) dt \tag{2}$$

$$n \int_0^{\frac{T_s}{2}} i_{Lr} dt \frac{V_0 T_s}{2 R_L} = 0 \tag{3}$$

$$\int_0^{\frac{T_s}{2}} i_{Lr} dt = \int_0^{\frac{T_s}{2}} C_r \frac{dv_{C_r} dt}{dt} = C_r \left(V_{c_{r_3}} - V_{c_{r_1}} \right) \tag{3}$$

$$\Delta V_0 = \frac{n C_r (V_{Cr3} - V_{Cr1})}{C_0} - \frac{V_0 T_s}{2 R_L C_0} \tag{5}$$

$$\begin{cases} i_{Lr1} = I_{Lrp1} \sin(\omega_0 t + \varphi_1) \big|_{mode1} \\ i_{Lr2} = I_{Lrp2} \sin(\omega_0 t + \varphi_2) \big|_{mode2} \end{cases} \tag{6}$$

$$\begin{cases} I_{Lrp1} = \sqrt{\frac{(V_{Cr1} - x_1)^2}{Z_0^2 + (-I_{Lm})^2}} \\ \\ I_{Lrp2} = \sqrt{\frac{(V_{Cr2} - x_2)^2}{Z_0^2 + (-I_{Lr})^2}} \\ \\ V_{Cr2} = I_{Lrp1} Z_0 \cos(\omega_0 t_{12} + \varphi_1) + x_1 \end{cases} \tag{7}$$

$$\left(\omega_0 = \frac{1}{\sqrt{L_r C_r}} \right) \tag{8}$$

$$\begin{cases} I_{Lrp1} \sin \varphi_1 = -I_{Lm} \\ I_{Lr2} = I_{Lrp1} \sin(\omega_0 t_{12} + \varphi_1) = I_{Lrp2} \sin \varphi_2 \\ I_{Lrp1} \sin(\omega_0 t_{23} + \varphi_2) = I_{Lm} \end{cases} \tag{9}$$

In between the time interval t_{01} and t_{02}, the time is equal to half of the switching period T_s. The mathematical formula for this case is shown in Eq. (10). The freewheeling period of the rectifier diode is represented using the notation t_{01} and it is equal to $t_{23-last}$, which is the freewheeling period of the previous mode. These help in evaluating the entire variables required for switching and further the term V_{Cr3} is evaluated as ΔV_0 and the mathematical formula for V_{Cr3} is shown in Eq. (11). In the iteration method, the state variables are measured by fixing $V_0 = V_{Cr} = I_{Lr1} = I_{Lm} = t_{01} = 0$ and in mode 1 or 3, the values of L_{rp1}, ϕ_1 and t_{12}, V_{Cr2} are computed. In mode 2 or 4, the values of L_{rp2}, ϕ_2 and t_{23}, V_{Cr3} are computed. Then, the value of $\Delta V_0, V_0, I_{Lm}$ is computed and once if the steady-state is reached, the obtained values are the state variables and in case of not reaching the steady-state, the value of $t_{01} = t_{23}$ and $V_{Cr1} = V_{Cr3}$ are assumed and the process is repeated.

$$t_{01} + t_{02} = \frac{T_s}{2} \tag{10}$$

$$V_{Cr3} = I_{Lrp2} Z_0 \cos(\omega_0 t_{23} + \varphi_2) + x_2 \tag{11}$$

4.2 Peak Value of Resonant Current

At lower switching frequency, the resonant current has reached the peak value and it resembles the amplitude of resonant current and when the frequency of switching is greater at the final moment. When the switching is greater at the final moment value and it is equivalent to the resonant current value of mode 1 and mode 3. The output voltage at the starting instant is equal to zero and hence the value of $x_1 = x_4 = V_{in}, x_2 = x_3 = 0$. Here, mode 2 and mode 4 are lessened. Eq. (12) depicts the circular trajectory in radian throughout the entire mode of operation. The term $i_{Lr1}, i_{Lr2}, i_{Lr3}$ tells about the resonant current in each model at the finishing point and the normalized frequency is referred to as f_n and it is $f_n = f / f_r$

$$\alpha_1 = \omega_0 \frac{T_s}{2} = \frac{\pi}{f_n} \tag{12}$$

The mathematical formula for resonant current's peak value in the initial switching duration is exhibited in Eq. (13). The input resistor and the output voltage is denoted using the term R_1 and V_{in}, respectively. In Eq. (14) and Eq. (15), $i_{Lr1} < \frac{R_1}{Z_0} < i_{Lr3} < i_{Lr2} < \frac{R_2}{Z_0}$ and the vertex angle is denoted as θ_2.

$$I_{Lrm} = i_{Lr1} = \frac{R_1}{Z_0} \sin\left(\frac{\omega_0 T_s}{2}\right) = \frac{V_{in}}{Z_0} \sin\left(\frac{\pi}{f_n}\right)(f_n > 2) \tag{13}$$

$$R_2 = 2R_1 \sin\left(\frac{\alpha_1}{2}\right) = 2V_{in} \sin\frac{\omega_0 T_s}{4} = 2V_{in} \sin\left(\frac{\pi}{2f_n}\right) \tag{14}$$

$$I_{Lrm} = i_{Lr2} = \frac{R_2}{Z_0} \sin(\alpha_1 - \theta_2) = \frac{R_2}{Z_0} \sin\left(\alpha_1 - \left(\frac{\pi}{2} - \frac{\alpha_1}{2}\right)\right) \tag{15}$$

$$I_{Lrm} = \frac{V_{in}}{Z_0} \sin\left(\frac{\pi}{f_n}\right) - \sin\left(\frac{2\pi}{f_n}\right) \quad (1.5 < f_n \leq 2) \tag{16}$$

5. Objective Function of LLC Converter Design

5.1 Objective Function and Solution Encoding

The major objective of this research is to diminish the error function G, which is the total error e^* between the error measurement e_1 and error measurement e_2. The error measurement e_1 is the error between the output voltage V_0 and the desired output voltage V_0^D. The error measurement e_2 is the difference between the peak value of resonant current I_{Lrm} and the desired peak value of resonant current I_{Lrm}^D. The mathematical formula for error measurement e_1 and the error measurement e_2 is shown in Eq. (21) and Eq. (22), correspondingly. The mathematical formula for total error measurement e^* is the addition of the errors e_1 and e_2 as per Eq. (19). Further, Eq. (20) depicts the mathematical formula for the error function G.

$$e_1 = \left(V_0^D - V_0\right) \tag{17}$$

$$e_1 = \left(I_{Lrm}^D - I_{Lrm}\right) \tag{18}$$

$$e^* = e_1 + e_2 \tag{19}$$

$$G = Min\left(e^*\right) \tag{20}$$

The solutions C_r, L_r, ϕ and τ are encoded for obtaining the objective function (i.e., attaining minimum I_{Lrm} and V_0 values). The term C_r, L_r, ϕ and τ depicts the resonant capacitor, resonant inductor, angle of the initial point and frequency time constant, respectively. The lower limit of C_r is e^{-6} and the upper limits is $100e^{-6}$. The lower limit of L_r is e^{-9} and the upper limit is $5e^{-9}$. The upper limit and the lower limit of ϕ is 1 and e^3, respectively and the lower limit and upper limits of τ are 1 and 100 respectively. The diagrammatic representation of the solution encoding is shown in Fig. 2.
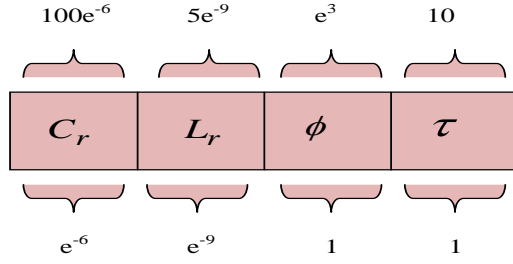
Fig. 2. *Solution encoding process*

5.2 Standard Firefly Algorithm

As mentioned before, the solutions such as C_r, L_r, ϕ and τ are optimized using FF algorithm [35] and [36]. This algorithm was introduced in the year 2008 by Xin-She. Three major assumptions of FF are (a) (a) all FF are unisex (b) Attractiveness ρ of FF α brightness and Attractiveness of FF α 1/ distance between fireflies. (c) The brightness of FF is defined in terms of the objective function. The attractiveness of FF is denoted as ρ is directly proportional to distance x. The mathematical formula for attractiveness between two EE is shown in Eq. (17), in which the maximum attractiveness (light absorption coefficient) is denoted as ρ_0. In addition, K_g is the position of gth FF and K_h is the position of hth FF. Then, Eq. (18) depicts the mathematical formula for the distance between two FF, in which the notation b is the count of the dimensions. Eq. (23) depicts the movement of FF and on the basis of the distance between FF; the value of M_h (light intensity) is measured. The initial position of FF is denoted as per Eq. (24), in which the first term tells about the current position of FF, the second term portrays the attractiveness of FF and the last term depicts the random movement of FF. The represents the original light intensity is depicted using the term M_0. The pseudo-code for conventional FF is shown in Algorithm 1.

$$M = M_0 e^{-\gamma x} \tag{21}$$

$$\rho(x) = \rho_0 e^{-\gamma x} \quad , v \geq 1 \tag{22}$$

$$x_{gh} = \left\| K_g - K_h \right\| = \sqrt{\sum_{w=1}^{b} (K_{g,w} - K_{h,u})^2} \tag{23}$$

$$K_{best} = K_g + \rho_0^{-\gamma x_{gh}^2} (K_h - K_g) + \omega \left(rand - \frac{1}{2} \right) \tag{24}$$

Algorithm 1: Firefly algorithm

Initialize Maximum generation Max_g and intensity of light M_g

Light absorption co-efficient is defined

While $(t < Max_g)$

For $g = 1 : n_1$ for all FF

    For $h = 1 : n_2$ for all FF

        If $(M_h > M_g)$

            FF g is moved towards h

        End if

        Attractiveness varies with distance x

        New solutions are evaluated and light intensity is updated

    End for h

End for g

FF are ranked and the best FF is predicted

End while

Thus by adopting FF technique, the parameters such as I_{Lrm} and V_0 can be minimized by optimizing the relevant parameters.

6. Results and Discussions

6.1 Simulation Procedure

The proposed LCR-RC model on the basis of the FF-PO algorithm was simulated in MATLAB, and the optimal results were obtained. In this experiment, the value of I_{Lrm} and V_0 are optimized and the steady-state response is recorded. It was analyzed for three different experiments by fixing the set points of (I_{Lrm}, V_0) at (15, 23), (5, 20) and (10, 25), respectively for experiment 1, experiment 2 and experiment 3, respectively. The proposed FF-PO model was compared with other conventional models like IA-PO [35], ABC-PO [31], PSO-PO [32], WOA-PO [33] and GWO-PO [34].

6.2 Error Analysis

RMSE of the proposed FF-PO model for LLC-RC for three set points namely, (15, 23), (5, 20) and (10, 25) for I_{Lrm} and V_0 is shown in Fig. 3(a) and Fig. 3(b), respectively. Fig. 3(a) depicts the RMSE values obtained by varying I_{Lrm} for three set points namely, (15, and 23), (5, 20) and (10, 25). For the first experiment (Experiment -1), the value of FF-PO is 92% and 51% better than IA-PO and ABC-PO techniques, respectively. In the second experiment (Experiment-2), the proposed FF-PO model in terms of RMSE for varying I_{Lrm} is 29.8% and 14% better than the traditional PSO-PO and FFPO technique. In Experiment-3, the RMSE of the proposed FF-PO model is 94.7% superior to IA-PO and 73% superior to GWO-PO technique. Thus, from this analysis on RMSE values for varying I_{Lrm}, the proposed FF-PO model exhibits better performance.

Fig. 3(b) illustrates the RMSE values obtained by varying V_0 for three experiments (Experiments -1, Experiment -2, and Experiment-3) for three set points namely, (15, 23), (5, 20) and (10, 25), respectively. RMSE value of the proposed FF-PO for Experiment-1 is 59.8% and 3.8% better than the state-of-art model like IA-PO and ABC-PO techniques, respectively. In Experiment-2, RMSE value of the proposed FF-PO model is 35.7% better than PSO-PO and 14.2% better than GWO-PO, respectively. In Experiment-3, the proposed FF-PO method is 45.8% superior to IA-PO and 20.6% superior to GWO-PO techniques. Thus, from this analysis on RMSE values for varying V_0, the proposed FF-PO model exhibits better performance.
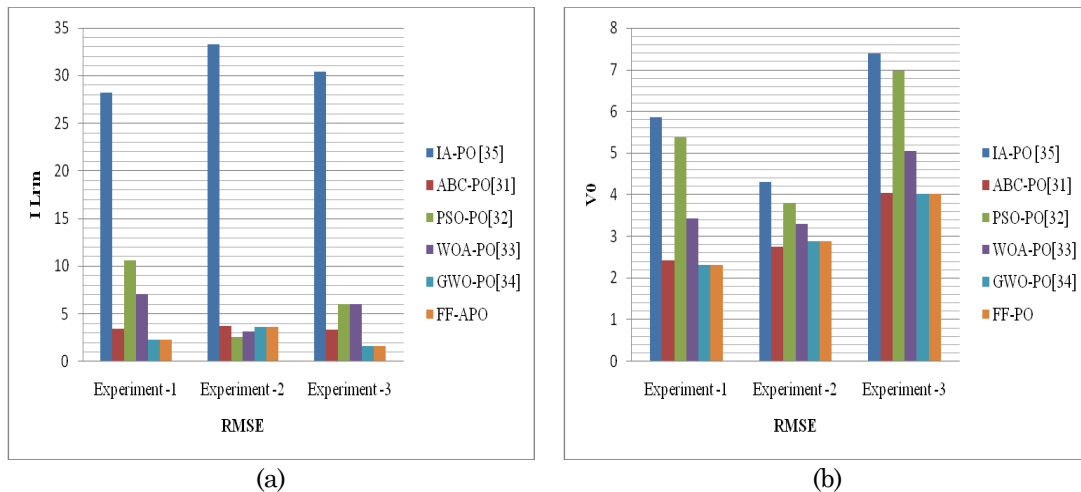

(a)   (b)

Fig. 3. *Graphical representation of RMSE value obtained by varying (a)* I_{Lrm} *(b)* V_0

6.3 Analysis of the Steady-State Response

The proposed FF-PO model is analysed in terms of , rise time, settling time, settling minimum, settling maximum, overshoot, undershoot, peak and peak time for three different experiments by fixing the set points of (I_{Lrm}, V_0) at (15, 23), (5, 20) and (10, 25), respectively. Table 1 depicts the steady-state response I_{Lrm} corresponding to Experiment -1. From the analysis, it is clear that the Settling Time is lowest in the proposed model FF-PO and the corresponding value is 8.555574. The setting time of the conventional models like IA-PO, ABC-PO, PSO-PO, WOA-PO, and GWO-PO is 45.98023, 17.779576, 23.71366, 16.371086 and 8.557208, respectively. The minimum Settling time is achieved by FF-PO as 5.002178. Table 2 depicts the corresponding values of V_0 for different experiments. The minimum setting level is low in the proposed FF-PO model and it is 10.47603, the other levels are 12.54166, 14.50717, 18.54166,

13.03174, and 12.48852 for IA-PO, ABC-PO, PSO-PO, WOA-PO, and GWO-PO, respectively. The overshoot value of the proposed FF-PO model is 0.107007 and the peak value is 12.9905. Table 3 show casts the steady-state analysis for I_{Lrm} for Experiment-2. The rise time=0 for both the proposed as well as the existing model. The lowest Settling Time is 7.77782 and it is achieved in proposed FF-PO. The Settling Minimum has the lowest value as 5.000397 and the setting max value as 22.70768 for the proposed FF-PO model. The Overshoot and the Undershoot value of proposed FF-PO model are 554.1017 and 1.835594, correspondingly. Table 4 exhibits the steady-state V_0 analysis for Experiment-2 in which the Settling Time of FF-PO is 13.15255 and it is 54.45%, 11.9%, 49.48%, and 0.02% better than IA-PO, ABC-PO, PSO-PO, WOA-PO, and GWO-PO, respectively. Table 5 exhibits the steady-state analysis for I_{Lrm} Experiment-3, from which the overshoot of the proposed FF-PO model is 47.58612, which is 88.8% better than IA-PO, 34.9% better than ABC-PO, 83.3% better than WOA-PO and 85.2% better than GWO-PO. Table 6 depicts the steady-state analysis for V_0 regarding Experiment-3. Here, the value of Settling Time for the proposed FF-PO model is 8.962245 and it is 47.5%, 51.6%, 44.3%, 32%, and 0.7% better than existing than IA-PO, ABC-PO, PSO-PO, WOA-PO, and GWO-PO, respectively.

Table 1. *Analysis of Steady-state Stability for* I_{Lrm} *for 1st experiment*

Methods	IA-PO [35]	ABC-PO [31]	PSO-PO [32]	WOA-PO [33]	GWO-PO [34]	FF-PO
Rise time	0	0	0	0	0	0
Settling Time	45.98023	7.779576	23.71366	6.371086	8.557208	8.555574
Settling Min	3.902498	15.19063	3.902498	1.506247	5.111981	5.002178
Settling Max	59.58278	18.57222	22.83132	74.93567	24.59467	24.40701
Overshoot	1426.785	20.57158	485.0438	501.9619	63.96446	62.73971
Undershoot	0	74.29702	0	20.42285	0	0
Peak	59.58278	18.57222	22.83132	74.93567	24.59467	24.40701
Peak Time	45	6	3	3	3	3

Table 2. *Analysis of Steady-state Stability for* V_0 *for 1st experiment*

Methods	IA-PO [35]	ABC-PO [31]	PSO-PO [32]	WOA-PO [33]	GWO-PO [34]	FF-PO
Rise time	0	0	0	0	0	0
Settling Time	7.09298	4.512533	6.10274	7.12522	3.065112	2.107312
Settling Min	12.54166	14.50717	18.54166	13.03174	12.48852	10.47603
Settling Max	19.52631	13.2531	20.52631	33.48649	22.98853	12.9905
Overshoot	0	0.001192	0	61.10978	0.106135	0.107007
Undershoot	0	0	0	0	0	0
Peak	10.52631	13.2531	10.52631	23.48649	12.98853	12.9905
Peak Time	100	12	100	2	6	6

Table 3. *Analysis of Steady-state Stability for* I_{Lrm} *for 2nd experiment*

Methods	IA-PO [35]	ABC-PO [31]	PSO-PO [32]	WOA-PO [33]	GWO-PO [34]	FF-PO
Rise time	0	0	0	0	0	0
Settling Time	35.98023	8.65921	14.78616	8.01649	9.77991	7.77782
Settling Min	3.902498	5.250561	4.285375	4.997268	4.999946	5.000397
Settling Max	49.58278	24.28264	10.06399	16.51892	22.70482	22.70768
Overshoot	1426.785	552.9328	368.1968	430.6683	554.1035	554.1017
Undershoot	0	3.117753	0	0	1.833235	1.835594
Peak	39.58278	14.28264	8.06399	16.51892	12.70482	12.70768
Peak Time	45	3	3	3	3	3

Table 4. *Analysis of Steady-state Stability for* V_0 *for 2nd experiment*

Methods	IA-PO [35]	ABC-PO [31]	PSO-PO [32]	WOA-PO [33]	GWO-PO [34]	FF-PO
Rise time	0	0	0	0	0	0
Settling Time	27.09298	11.75384	25.88162	17.8867	13.15562	13.15255
Settling Min	18.54166	18.59842	19.03922	18.89421	18.64038	18.64128
Settling Max	20.52631	20.17241	21.02916	20.96248	20.17241	20.17241
Overshoot	0	0	0	0	0	0
Undershoot	0	0	0	0	0	0
Peak	20.52631	20.17241	21.02916	20.96248	20.17241	20.17241
Peak Time	100	100	100	100	100	100

Table 5. *Analysis of Steady-state Stability for* I_{Lrm} *for 3rd experiment*

Methods	IA-PO [35]	ABC-PO [31]	PSO-PO [32]	WOA-PO [33]	GWO-PO [34]	FF-PO
Rise time	0	0	0	0	0	0
Settling Time	25.98023	8.459763	13.71366	7.482513	8.16852	6.06433
Settling Min	3.902498	20.13032	13.902498	-9.58209	25.007195	5.22978
Settling Max	39.58278	17.80458	10..83132	42.32365	6.78018	6.77473
Overshoot	426.785	73.1331	285.0438	323.2078	47.80226	47.58612
Undershoot	0	0	0	95.81646	0	0
Peak	59.58278	37.80458	22.83132	62.32365	16.78018	16.77473
Peak Time	45	3	3	3	6	6

Table 6. *Analysis of Steady-state Stability for* V_0 *for 3rd experiment*

Methods	IA-PO [35]	ABC-PO [31]	PSO-PO [32]	WOA-PO [33]	GWO-PO [34]	FF-PO
Rise time	0	0	0	0	0	0
Settling Time	17.09298	5.911161	16.10274	13.369537	9.029978	8.962245
Settling Min	8.54166	10.25554	8.54166	10.18556	10.76239	10.7993
Settling Max	10.52631	12.1793	10.52631	11.8122	12.72726	12.72052
Overshoot	0	7.29E-09	0	6.009367	0	0
Undershoot	0	0	0	0	0	0
Peak	10.52631	12.1793	10.52631	11.8122	12.72726	12.72052
Peak Time	100	29	100	2	76	75

7. Conclusion

This paper projected an LLC-RC design model by means of optimizing the parameters like output voltage and resonant inductor current with the help of FF-PO model. The proposed model reduced the error of the system. The modified design in the optimization process was updated using FF-PO model. Finally, the proposed FF-PO model was compared with existing methods like IA-PO, ABC-PO, PSO-PO, WOA-PO, and GWO-PO in terms of error and steady-state analysis by varying I_{Lrm} and V_0. The value of Settling Time for the proposed FF-PO model for Experiment- 3 is 8.962245 and it is 47.5%, 51.6%, 44.3%, 32%, and 0.7% better than existing than IA-PO, ABC-PO, PSO-PO, WOA-PO, and GWO-PO, respectively.

References

[1] Min-Jun Kwon,Woo-Cheol Lee,"No-Load Control Method of LLC Resonant Converter for Plasma Sputtering Process Using Full-Bridge Structure",Journal of Electrical Engineering & Technology,col.14, no.2,pp.pp 795–803,March 2019.

[2] Amit Kumar Singh,"A SQR Based High Voltage LLC Resonant DC–DC Converter", Analysis and Design of Power Converter Topology, 2018.

[3] M. Madheswaran,C. Nagarajan,"DSP based fuzzy controller for series parallel resonant converter",Frontiers of Electrical and Electronic Engineering,vol.7, no.4, pp 438–446,December 2012.

[4] Chih-Chiang Hua, Yung-Lin Deng,"A Novel Dual-Bridge LLC Resonant Converter with Wide Range of Low Input Voltage",Energy Procedia,vol.156,pp.361-365,January 2019.

[5] Dongjiang Yang, Bin Duan, Wenlong Ding, Jinqiu Song, Chenghui Zhang,"A bidirectional LLC-C Resonant DC-DC Converter Based on Normalized Symmetry Resonant Tank",IFAC-PapersOnLine, vol.15,no.31,pp.685-689,2018.

[6] Hui-pin Lin, Xiao-guang Jin, Liang Xie, Jin Hu and Zheng-yu Lu, "A new variable-mode control strategy for LLC resonant converters operating in a wide input voltage range", vol. 18, no. 3, pp. 410–422, March 2017.

[7] X. Fang et al., "Efficiency-Oriented Optimal Design of the LLC Resonant Converter Based on Peak Gain Placement,"IEEE Transactions on Power Electronics, vol. 28, no. 5, pp. 2285-2296, May 2013.

[8] [8] X. Fang, H. Hu, Z. J. Shen and I. Batarseh, "Operation Mode Analysis and Peak Gain Approximation of the LLC Resonant Converter, "IEEE Transactions on Power Electronics, vol. 27, no. 4, pp. 1985-1995, April 2012.

[9] R. Yu, G. K. Y. Ho, B. M. H. Pong, B. W. K. Ling and J. Lam, "Computer-Aided Design and Optimization of High-Efficiency LLC Series Resonant Converter, "IEEE Transactions on Power Electronics, vol. 27, no. 7, pp. 3243-3256, July 2012.

[10] G. Ivensky, S. Bronshtein and A. Abramovitz, "Approximate Analysis of Resonant LLC DC-DC Converter, "IEEE Transactions on Power Electronics, vol. 26, no. 11, pp. 3274-3284, Nov. 2011.

[11] R. L. Steigerwald, "A comparison of half-bridge resonant converter topologies,"IEEE Transactions on Power Electronics, vol. 3, no. 2, pp. 174-182, Apr 1988.

[12] M. P. Foster, C. R. Gould, A. J. Gilbert, D. A. Stone and C. M. Bingham, "Analysis of CLL Voltage-Output ResonantConverters Using Describing Functions,"IEEE Transactions on Power Electronics, vol. 23, no. 4, pp. 1772-1781, July 2008.

[13] J. F. Lazar and R. Martinelli, "Steady-state analysis of the LLC series resonant converter," APEC 2001. Sixteenth Annual IEEE Applied Power Electronics Conference and Exposition (Cat. No.01CH37181), vol.2, pp. 728-735, 2001.

[14] P. Kowstubha, K. Krishnaveni and K. Ramesh Reddy, "Performance analysis of pulse analog control schemes for LLC resonant DC/DC converters suitable in portable applications", Journal of Electrical Systems and Information Technology, vol. 3, no. 3, pp. 454-470, December 2016.

[15] G. De Falco, M. Riccio, G. Breglio and A. Irace, "Thermal-aware design and fault analysis of a DC/DC parallel resonant converter", Microelectronics Reliability, vol. 54, no. 9–10, pp. 1833-1838, 2014.

[16] F. Giri, O. El Maguiri, H. El Fadil and F.Z. Chaoui, "Nonlinear adaptive output feedback control of series resonant DC–DC converters", Control Engineering Practice, vol. 19,no. 10, pp. 1238-1251, October 2011.

[17] Chengchan Kaewanuchit, "Small – Signal Model of Series – Parallel Resonant DC-DC Converter with Capacitive Output Filter", Procedia Engineering, vol. 8, pp. 42-46, 2011.

[18] U. Kundu; P. Sensarma, "A Unified Approach for Automatic Resonant Frequency Tracking in LLC DC-DC Converter,"IEEE Transactions on Industrial Electronics, vol.PP, no.99, pp.1-1, 2017.

[19] H. Wang, Y. Chen, Y. F. Liu, J. Afsharian and Z. Yang, "A Passive Current Sharing Method With Common Inductor Multiphase LLC Resonant Converter,"IEEE Transactions on Power Electronics, vol. 32, no. 9, pp. 6994-7010, Sept. 2017.

[20] J. H. Jung, H. S. Kim, M. H. Ryu and J. W. Baek, "Design Methodology of Bidirectional CLLC Resonant Converter for High-Frequency Isolation of DC Distribution Systems,"IEEE Transactions on Power Electronics, vol. 28, no. 4, pp. 1741-1755, April 2013.

[21] W. Chen, P. Rong and Z. Lu, "Snubberless Bidirectional DC–DC Converter With New CLLC Resonant Tank Featuring Minimized Switching Loss,"IEEE Transactions on Industrial Electronics, vol. 57, no. 9, pp. 3075-3086, Sept. 2010.

[22] J. W. Kim, J. K. Han and J. S. Lai, "APWM adapted half-bridge LLC converter with voltage doubler rectifier for improving light load efficiency,"Electronics Letters, vol. 53, no. 5, pp. 339-341, 3 2 2017.

[23] W. Sun, H. Wu, H. Hu and Y. Xing, "Modified LLC resonant converter with secondary paralleled bidirectional switch for applications with hold-up time requirement,"IET Power Electronics, vol. 10, no. 3, pp. 398-404, 2017.

[24] A. K. Singh, P. Das and S. K. Panda, "Analysis and Design of SQR-Based High-Voltage LLC Resonant DC–DC Converter,"IEEE Transactions on Power Electronics, vol. 32, no. 6, pp. 4466-4481, June 2017.

[25] H. Wang, Y. Chen, P. Fang, Y. F. Liu, J. Afsharian and Z. Yang, "An LLC Converter Family With Auxiliary Switch for Hold-Up Mode Operation,"IEEE Transactions on Power Electronics, vol. 32, no. 6, pp. 4291-4306, June 2017.

[26] J. W. Kim, J. P. Moon and G. W. Moon, "Duty-Ratio-Control-Aided LLC Converter for Current Balancing of Two-Channel LED Driver,"IEEE Transactions on Industrial Electronics, vol. 64, no. 2, pp. 1178-1184, Feb. 2017.

[27] T. Mishima, H. Mizutani and M. Nakaoka, "A Sensitivity-Improved PFM LLC Resonant Full-Bridge DC–DC Converter With LC Antiresonant Circuitry,"IEEE Transactions on Power Electronics, vol. 32, no. 1, pp. 310-324, Jan. 2017.

[28] J. B. Lee, J. K. Kim, J. I. Baek, J. H. Kim and G. W. Moon, "Resonant Capacitor On/Off Control of Half-Bridge LLC Converter for High-Efficiency Server Power Supply,"IEEE Transactions on Industrial Electronics, vol. 63, no. 9, pp. 5410-5415, Sept. 2016.

[29] S. Zong, H. Luo, W. Li, Y. Deng and X. He, "Asymmetrical Duty Cycle-Controlled LLC Resonant Converter With Equivalent Switching Frequency Doubler,"IEEE Transactions on Power Electronics, vol. 31, no. 7, pp. 4963-4973, July 2016.

[30] F. Duan, M. Xu, X. Yang and Y. Yao, "Canonical Model and Design Methodology for LLC DC/DC Converter With Constant Current Operation Capability Under Shorted Load,"IEEE Transactions on Power Electronics, vol. 31, no. 10, pp. 6870-6883, Oct. 2016.

[31] P. Shunmugapriya, S. Kanmani, "A hybrid algorithm using ant and bee colony optimization for feature selection and classification (AC-ABC Hybrid)", Swarm and Evolutionary Computation, vol. 36, pp. 27-36, October 2017.

[32] Nandar Lynn, Ponnuthurai Nagaratnam Suganthan, "Ensemble particle swarm optimizer", Applied Soft Computing, vol. 55, pp. 533-548, June 2017.

[33] Seyedali Mirjalili, Andrew Lewis, "The Whale Optimization Algorithm", Advances in Engineering Software, vol. 95, pp. 51-67, May 2016.

[34] Abdul Kayom Md Khairuzzaman, Saurabh Chaudhury, "Multilevel thresholding using grey wolf optimizer for image segmentation", Expert Systems with Applications, vol. 86, pp. 64-76, 15 November 2017.

[35] R. Zheng, B. Liu and S. Duan, "Analysis and Parameter Optimization of Start-Up Process for LLC Resonant Converter,"IEEE Transactions on Power Electronics, vol. 30, no. 12, pp. 7113-7122, Dec. 2015.

[36] G Singh, V K Jain, A Singh, "Adaptive network architecture and firefly algorithm for biogas heating model aided by photovoltaic thermal greenhouse system",Energy & Environment, vol. 29 (7), pp.1073-1097, 2018.